Cancer Research

Bridging Population and Tissue Scale Tumor Dynamics: A New Paradigm for Understanding Differences in Tumor Growth and Metastatic Disease

Jill Gallaher[1], Aravind Babu[2], Sylvia Plevritis[3], and Alexander R.A. Anderson[1]

Abstract

To provide a better understanding of the relationship between primary tumor growth rates and metastatic burden, we present a method that bridges tumor growth dynamics at the population level, extracted from the SEER database, to those at the tissue level. Specifically, with this method, we are able to relate estimates of tumor growth rates and metastatic burden derived from a population-level model to estimates of the primary tumor vascular response and the circulating tumor cell (CTC) fraction derived from a tissue-level model. Variation in the population-level model parameters produces differences in cancer-specific survival and cure fraction. Variation in the tissue-level model parameters produces different primary tumor dynamics that subsequently lead to different growth dynamics of the CTCs. Our method to bridge the population and tissue scales was applied to lung and breast cancer separately, and the results were compared. The population model suggests that lung tumors grow faster and shed a significant number of lethal metastatic cells at small sizes, whereas breast tumors grow slower and do not significantly shed lethal metastatic cells until becoming larger. Although the tissue-level model does not explicitly model the metastatic population, we are able to disengage the direct dependency of the metastatic burden on primary tumor growth by introducing the CTC population as an intermediary and assuming dependency. We calibrate the tissue-level model to produce results consistent with the population model while also revealing a more dynamic relationship between the primary tumor and the CTCs. This leads to exponential tumor growth in lung and power law tumor growth in breast. We conclude that the vascular response of the primary tumor is a major player in the dynamics of both the primary tumor and the CTCs, and is significantly different in breast and lung cancer. *Cancer Res; 74(2); 426–35. ©2013 AACR.*

Major Findings

By bridging a population-scale model to a tissue-scale model of tumor dynamics, we have identified the vascular response as a primary cause for the differences in tumor growth rates and metastatic disease between two common cancers: breast and lung cancer.

Introduction

Mathematical models of tumor growth and progression have been developed at both the population and tissue scales, but rarely have these 2 scales been connected. This disconnect is not surprising given the varied scope of interactions dominating each scale. However, the ability to infer tumor growth dynamics that are consistent at both scales promises to enrich our understanding of disease progression and improve our predictions of treatment response and outcomes. Historically, growth dynamics were studied by picking an appropriate growth law, from exponential to power law to Gompertzian, to provide better fits with tumor growth data, but often the causative factors for differences in growth behavior are not identified (1). Although establishing the underlying drivers of tumor growth dynamics has always been a persistent objective in cancer research, frequently the focus is on a specific aspect on a specific scale. To get a handle on the causative factors, we need to dig a little deeper and examine this growth in a more mechanistic and systematic fashion.

We are interested in relating the growth of the primary tumor to the likelihood of survival from metastatic burden. We recognize that there is a complex path from neoplasm to advanced disease that involves many steps: primary growth, local invasion, entrance to and survival within the bloodstream, evasion of the immune system, and localization to a new target organ. Without taking into account all of these steps, we use a more comprehensive approach. Specifically, we connect the primary tumor growth dynamics to the metastatic

Authors' Affiliations: [1]Integrated Mathematical Oncology, Moffitt Cancer Center, Tampa, Florida; [2]Institute for Computational and Mathematical Engineering, Stanford University; and [3]Department of Radiology, Stanford University School of Medicine, Stanford, California

Note: Supplementary data for this article are available at Cancer Research Online (http://cancerres.aacrjournals.org/).

S. Plevritis and A.R.A. Anderson share senior authorship.

Corresponding Author: Jill Gallaher, Moffitt Cancer Center, 12902 Magnolia Dr., Tampa, FL 33612. Phone: 813-745-6087; Fax: 813-745-6497. E-mail: jill.gallaher@moffitt.org

doi: 10.1158/0008-5472.CAN-13-0759

Quick Guide to Equations and Assumptions

We construct our tissue-scale model from a system of one-dimensional PDEs that describe tumor growth radially and the corresponding metastatic burden based on the angiogenic cascade. There are 5 cell types: 4 states of tumor cells and the vasculature (cf. Fig. 2). The cells within the tumor can be normoxic (n), hypoxic (h), or necrotic (d). The circulating tumor cells (c) have left the primary site and reside in the greater vascular system. The local vasculature (ν) is also present and plays a significant role in determining the rates of flow between these compartments. This model is both a development and a simplification of the works of Swanson and colleagues (4) and Hinow and colleagues (5).

We start with a small (~3 mm diameter) initial lump of normoxic tumor cells and a constant vascular density (2%) throughout. Of the tumor cells, only the normoxic cells proliferate, and they do so at a rate μ_n proportional to the amount of vasculature present. They become hypoxic because of lack of vasculature at a rate α_n. Once hypoxic, the cells may reoxygenate at a rate α_h proportional to the vascular density or become chronically hypoxic, that is necrotic, at a rate δ_h. Normoxic cells and hypoxic cells enter the bloodstream at rates β_n and β_h, respectively, also proportional to the vascular density. The vascular density is itself influenced by a rate of proliferation and death, the former rate μ_ν being proportional to the hypoxic fraction and the latter with a rate of δ_ν. The dependence of vascular proliferation on the hypoxic cell density is an indirect consequence of vascular endothelial growth factor (VEGF) production by the hypoxic cells, which in turn stimulates vascular growth (6), that is the angiogenic response. Production of proliferating cells is stifled by the term $(1-w)$ as the total density of cells in the tumor ($w = n + h + d + \nu$) approach the carrying capacity, which is scaled to 1.

There are additional spatially dependent interactions that cannot be represented in the compartment diagram of Fig. 2. The normoxic, hypoxic, and vascular cells all undergo random migratory dispersal. Also, the vascular cells have a chemotactic term that drives them up the gradient of hypoxic cells, mimicking a chemotactic response to higher concentrations of VEGF (which would naturally occur where the higher density of hypoxic cells exist). A system of coupled partial differential equations for the vascular cells and each type of tumor cell describes their change over time and space (cf. Eq. A).

Equations

For normoxic (n), hypoxic (h), necrotic (d), circulating (c), and vascular (ν) cells, the equations are:

$$\begin{aligned}
\frac{\partial n}{\partial t} &= D_n \underbrace{\frac{\partial^2 n}{\partial x^2}}_{\text{diffuse}} + \underbrace{\mu_n n\nu(1-w)}_{\text{proliferate}} + \underbrace{\alpha_h h\nu}_{\text{reoxygenate}} - \underbrace{\alpha_n n(1-\nu)}_{\text{deoxygenate}} - \underbrace{\beta_n n\nu}_{\text{extravsate}} - \underbrace{\delta_n n}_{\text{necrose}} \\
\frac{\partial h}{\partial t} &= D_h \underbrace{\frac{\partial^2 h}{\partial x^2}}_{\text{diffuse}} - \underbrace{\alpha_h h\nu}_{\text{reoxygenate}} + \underbrace{\alpha_n n(1-\nu)}_{\text{deoxygenate}} - \underbrace{\beta_h h\nu}_{\text{extravasate}} + \underbrace{\delta_h h}_{\text{necrose}} \\
\frac{\partial d}{\partial t} &= \underbrace{\delta_h h}_{\text{accumulate}} - \underbrace{\delta_h h}_{\text{expunge}} \\
\frac{\partial c}{\partial t} &= \underbrace{\beta_n n\nu}_{\text{from } n} + \underbrace{\beta_h h\nu}_{\text{from } h} \\
\frac{\partial \nu}{\partial t} &= D_\nu \underbrace{\frac{\partial^2 \nu}{\partial x^2}}_{\text{diffuse}} + \chi \underbrace{\frac{\partial}{\partial x}}_{\text{chemotax}} \left(\nu \frac{\partial h}{\partial x}\right) + \underbrace{\mu_\nu \nu h(1-w)}_{\text{proliferate}} - \underbrace{\delta_\nu \nu}_{\text{expunge}} .
\end{aligned} \tag{A}$$

The values n, h, d, c, and ν are expressed as densities representing the percentage of the local volume occupied. A backward finite difference method is used for solving the coupled PDEs, which is described in Supplementary Data Appendix 1.

Model assumptions

We assume in this model that there are 5 compartments representing distinct cell types. Although there is an obvious continuum between normoxia and hypoxia, we divide this range into just 2 qualitatively different cell types. As with all continuum models that are based on a PDE paradigm, the system is completely deterministic and assumes all compartments within a unit volume are equally mixed. All cells of the same type behave the same way, and only differences in density drive differences in dynamics. The maximum cell density within the tumor is assumed to be the same throughout.

Because the tumor is defined by a density of cells that can be diffuse at the leading edge, the border of the tumor is not well defined. Therefore, for all volume calculations, we define the tumor's leading edge to be where the normoxic cancer cells taper off

to occupy only 2% of the space. This number is somewhat arbitrary, but the slope is consistently steep enough that the volume will not vary much if another small value were taken. Tumor volumes are calculated assuming spherical symmetry. Measuring from the center of the tumor to this edge gives the radius (R), from which we find the primary tumor volume as $V = 4/3\pi R^3$.

To calculate the number of cells entering the circulation at each time point, we find the number of circulating cells present in the local volume by summing up concentric spherical shells at consecutive radial intervals. The total number of cells is the summation over all shells:

$$\text{CTCs} = \sum_i \frac{4}{3}\pi(x_{i+1}^3 - x_i^3)\frac{c_{i+1} + c_i}{2}\rho_0, \tag{B}$$

where x_i is the distance from the tumor's center, c_i is the relative density of cells subject to intravasation at that position, and ρ_0 is the average cellular density of the tumor. Under the assumption that all cells are 20-μm-diameter spheres and densely packed into the volume, we estimate this density as $\rho_0 \sim 10^8$ cells/cm^3. A running tab is kept as cells leave the local region at each time point and take residence in the blood as CTCs.

The tissue model assumes no self-seeding, death, extravasation, or growth of circulating cells within the bloodstream or as established metastases. This is only a consideration of those cells that have left the local region of the tumor, which is assumed to be proportional to the metastatic population. Because many of the parameters involving metastases cannot be experimentally measured, including additional variables and/or parameters here would only add further complexity with little concrete gain in our understanding. We therefore bypass many of these issues by the gross simplification that an increase in the number of CTCs shedding from the primary correlates with an increased risk of metastases.

burden utilizing 2 models: (i) a stochastic model at the population scale and (ii) a differential equation model at the tissue scale.

At the population level, we are able to look at large-scale trends from actual patient outcomes. From this perspective, we distinguish qualitative differences between 2 cancer types, namely breast and lung, and estimate tumor growth rates and patient survival rates. At the tissue level, we formulate a system of partial differential equations (PDE) to develop a spatio-temporal model of tumor growth and invasion. With this multiscale model approach, we can match the predicted growth dynamics from the population scale with those from the tissue scale. At the tissue scale, we can estimate the relative distributions of the different cell types at various stages of tumor growth to highlight differences between breast and lung cancer.

The population model is fit to data from patients with invasive ductal carcinoma (IDC) breast cancer and non–small cell lung cancer (NSCLC) from the NCI Surveillance Epidemiology and End Results (SEER) database (2). The SEER database collects and publishes cancer incidence and survival data from population-based cancer registries, including information such as patient demographics, primary tumor site, tumor morphology and stage at diagnosis, treatment, and follow-up for vital status. The basic scheme of the statistical population model is shown in Fig. 1. By using a Monte Carlo simulation model of clinical cancer-stage progression and fitting this model to the survival curves of 2 specific cancers, Lin and Plevritis obtained 2 metrics that will be used to calibrate the tissue-scale model. They estimated median tumor volume doubling times of 135 days for NSCLC and 252 days for IDC. In addition, cancer-specific cure fractions were estimated. The

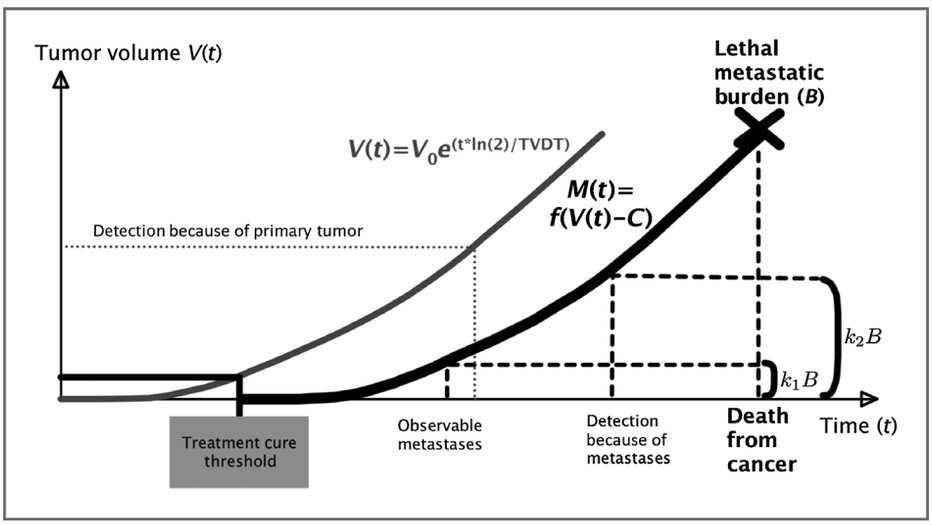

Figure 1. Stochastic population-level model diagram of cancer progression from previous work of Lin and Plevritis (3). The thin gray curve represents the growth of the primary tumor and the thick black curve represents the lethal metastatic burden. This same modeling framework is applied to both IDC and NSCLC SEER data. Reproduced with kind permission from Springer Science+Business Media: Cancer Causes and Control, Comparing the benefits of screening for breast cancer and lung cancer using a novel natural history model, 23, 2012, p. 176, Lin and Plevritis, Fig. 1.

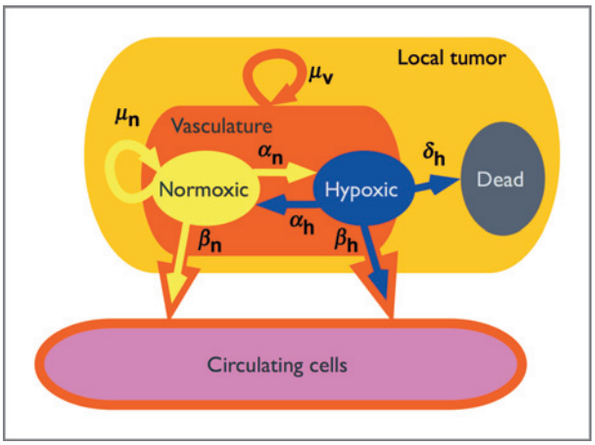

Figure 2. Schematic representation of the tissue model showing the interactions between the tumor components and the vasculature.

primary tumor size at which the likelihood of cure is at 50% (i.e., the point at which the tumor goes from likely to be cured to unlikely to be cured) occurs at diameters of 8 and 19 mm for NSCLC and IDC, respectively. Because this model has already been published, please see ref. 3 for further details. We will primarily focus on defining the tissue-scale model.

The contrasting trends of lung and breast cancers found from the statistical population model stimulates our inquiry: what are the major drivers of these very different responses? The population scale does not provide sufficient detail to answer this question, so we take a closer look at the tissue level to resolve the basic growth dynamics. We make the hypothesis that the differences are driven primarily by the degree of vascular response that the tumor elicits. Our rationale is that the close association of the lung tissue with the vasculature should contribute to faster, more efficient recruitment. The vasculature also necessarily connects the primary tumor to metastatic burden as the avenue for escape and translocation.

Materials and Methods

Using appropriate parameterizations for the PDE model, we match the estimates of the statistical population model for tumor volume doubling time and metastatic burden for both breast and lung. There are several parameters that are more significant for making the tissue growth dynamics fit the population-scale metrics. First, we adjust the migration of normoxic cells (D_n) and the proliferation of normoxic cells (μ_n) to set a baseline growth rate. Second, we set the rate that cells leave the tumor from the normoxic population (β_n) and the hypoxic population (β_h) to approximate the growth of the circulating tumor cell population. This is an obvious start for a loose fit, but we want to understand how differences in vascular interactions lead to different dynamics. So, given a base fit to dynamics that lie somewhere in between those of the breast tumor and those of the lung tumor, we inspect which parameters most significantly allow switching between the two. Rigorous parameter optimization is not the intent of this particular analysis, but it is rather to demonstrate 2 divergent behaviors. However, further analysis of the parameter space is presented in Supplementary Data Appendix 2 for a more detailed illustration of the system dynamics.

Results

We find that there are 3 parameters that most significantly affect switching from one tumor growth dynamic to the other: the vascular proliferation rate (μ_v), the rate of deoxygenation (α_n), and the rate of reoxygenation (α_h). Both α_n and α_h are scaled together, so they will collectively be referred to as one parameter (α) as a representation of the rate of switching between well-oxygenated and hypoxic cell states. We define all other parameters as constants to optimize the fits obtained when only these 2 parameters change. The values obtained were fit roughly and tabulated in Table 1.

Vascular response is a key driver for tumor growth differences

Upon fitting the tissue model to the estimates of the population model, we see a dramatic difference in vascular response and distribution at the end of 2.5 years (cf. Fig. 3). The breast tumor growth simulation in the left panel of Fig. 3 shows the normoxic cells growing outward followed by a swell of hypoxic cells. The vasculature responds to the increased hypoxic density by traveling up that gradient while the inner core becomes necrotic with time. This slower growing tumor shows the vasculature is taking up a maximum density of around 5% of the volume at the leading edge. The simulation of a tumor in lung tissue at the same time point is shown in the right panel of Fig. 3. In this case, the hypoxic population has overtaken the normoxic population throughout most of the tumor. This large hypoxic to normoxic ratio stimulates the vasculature to the point that it amounts to nearly half of the tumor volume. As a consequence, the tumor growth is much faster.

Limited vascular response leads to power law growth

Tumor volume over time for the breast and lung simulations is shown in Fig. 4. Each curve is fit to both an exponential function, that is $V = ae^{bt}$, and a power law function, that is $V = ct^n$. For the lung tumor simulation, exponential growth is a better fit, but for the breast tumor simulation, a power law fits better. It seems that with an adequate vascular response, as in the case of the lung tumor, unlimited exponential growth is supported, but a reduction of vascular activity comes with a limit on the growth, as seen in the breast tumor simulation.

To connect these growth rates to the statistical population model using 2 different growth trends, we need a common measure. Exponential growth has a constant tumor volume doubling time (TVDT), but power law growth will yield an increasing TVDT over time as the growth rate slows down. We therefore need to pick a relevant range of tumor volumes at which TVDT is usually measured for a good comparison. The method for obtaining TVDTs from breast and lung are outlined in Supplementary Data Appendix 3. These TVDTs per diameter are shown in the left panel of Fig. 5. Using Equation 2s in Supplementary Data at 3 cm, a typical tumor size from the

Table 1. The parameters used to fit the estimates for breast and lung tumor growth

Term	Parameter	Value	Scaled[a,b]
Diffusion	D_n	7.3×10^{-9} cm^2/s	7.0×10^{-5}
	D_h	1.7 D_n	1.2×10^{-4}
	D_v	0.8 D_n	5.6×10^{-5}
Proliferation	$\ln(2)/\mu_n$	16 h	1.04
	$\ln(2)/\mu_v$	60 h; 20 h	0.28; 0.83
Chemotaxis	χ	1.5×10^{-8} cm^2/s	1.4×10^{-4}
Conversion	α_n	6×10^{-5} h^{-1}; 4×10^{-3} h^{-1}	0.0014; 0.096
	α_h	$0.7\alpha_n$	0.0010; 0.067
	β_n	4.2×10^{-7} h^{-1}	1.0×10^{-5}
	β_h	7.8×10^{-7} h^{-1}	1.9×10^{-5}
Death	δ_n	1.0×10^{-5} h^{-1}	2.4×10^{-4}
	δ_h	7.0×10^{-5} h^{-1}	0.0017
	δ_v	1.0×10^{-5} h^{-1}	2.4×10^{-4}

NOTE: All parameters are the same for breast and lung tissues with the exception of those marked in gray; of those, the parameters for breast are listed first and those for lung are listed second.

[a]Timescale 24 h.

[b]Lengthscale 3 cm.

SEER dataset in the absence of screening, we get a TVDT of 237 days for the breast tumor simulation and 178 days for the lung tumor simulation. The constant TVDT using an exponential fit (Eq. 1s in Supplementary Data) is 153 days for the breast simulation and 143 days for the lung simulation. Recalling that the SEER data gave median TVDTs for breast as 252 days and lung as 135 days, for this metric, the power law fits the breast cancer data better and the exponential fits the lung cancer data better.

Metastatic burden correlation

Metastatic burden is an abstract concept that has the units of volume but does not take up any single particular continuous space. In the population model, it is a scaled version of the primary tumor in terms of volume and fits the SEER data nicely with an exponential function. The population model estimates, for breast and lung tumors, the size of the primary to a metastatic burden at which current treatment will be futile. Establishment of metastases is directly related to the number of tumor cells shed into the circulation (7, 8), and a larger number of circulating cells corresponds to a poorer prognosis (9). We parallel this in the tissue-scale model.

To connect the metastatic burden to the CTC fraction, we look to the literature. Studies by Cristofanilli and colleagues (10) and Budd and colleagues (11) establish a threshold of shorter progression-free and overall survival for patients having greater than 5 CTCs in 7.5 mL of blood with measurable metastatic breast cancer. Liu and colleagues (12) also demonstrates that this value holds as a good prognostic turning point both before and after initiation of therapy.

If we translate this value to a total CTC count well mixed within the ~5 L of blood in the human body, we get around 3,300 cells. This critical number at which the likelihood of survival reaches 50% is marked on the CTC population plot in the right panel of Fig. 5 by the top edge of the horizontal gray box. This edge indicates a switching point from local to advanced disease. It is clear from the simulation results that lung cancer achieves this threshold far more rapidly than breast cancer.

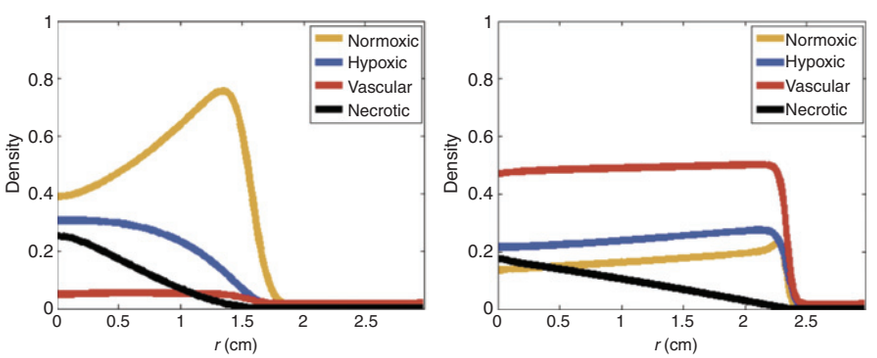

Figure 3. The distribution of cell types within the 2 tissue types at 2.5 years postinitiation. The legend details the colors for each cell type. The breast tumor (left) shows around 5% vascular content close to the edge, which is mostly occupied by normoxic cells, whereas the lung tumor (right) shows around 50% vascular content throughout and a large hypoxic fraction. The parameters for both cases are given in Table 1.

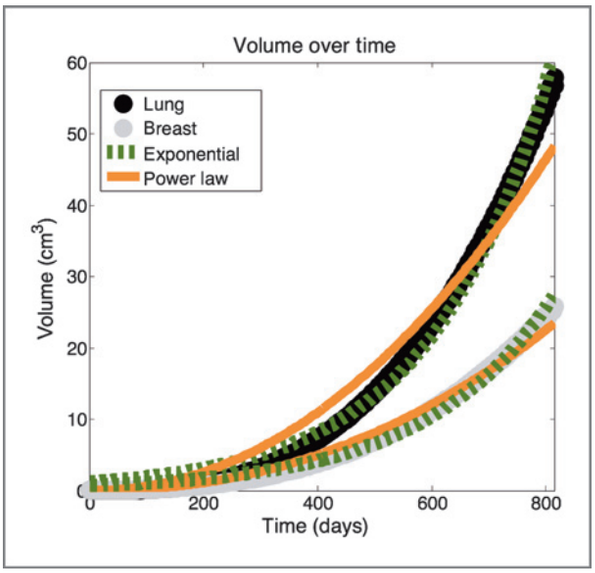

Figure 4. Tumor volume versus time for both lung (black) and breast (gray). The orange curves show power law fits ($N = at^n$) for lung with $a = 4.11 \times 10^{-5}$, $n = 2.09$, and $R = 0.978$ and breast with $a = 6.98 \times 10^{-6}$, $n = 2.24$, and $R = 0.995$. The green dashed curves show exponential fits ($N = ae^{bt}$) for the lung with $a = 1.17$, $b = 0.0049$ d^{-1}, and $R = 0.995$ and the breast with $a = 0.677$, $b = 0.0045$ d^{-1}, and $R = 0.994$. The breast simulation fits well to a power law, but the curve becomes more exponential-like with the vascular dynamics of the lung.

A closer look at parameter combinations

All parameters are fit to maximize the correlation of the 2 metrics, the TVDT and the diameter of the primary tumor when survival from the metastatic burden is 50%, by changing only the vascular proliferation rate, μ_v, and the deoxygenation–reoxygenation exchange rate, α. If we take a survey of the entire space of these 2 parameters, we get a clearer idea of how they combine with each other to affect the tumor's dynamics. The TVDT is shown in the left panel of Fig. 6 with the fits for the 2 tumors represented by planes (median values at 252 days for breast and 135 days for lung). The exponentially growing lung tumor is in the darkest region, and the slower growing breast tumor is in the lighter gray region. There are just a few parameter combinations that fit the lung tumor data: where α is large and μ_v is large [i.e., $\ln(2)/\mu_v$ is small]. The breast tumor, however, has several combinations of values that fit. The primary tumor diameter corresponding to the lethal CTC threshold is shown in the right panel of Fig. 6 within the same parameter space. Again, the fits to the 2 tumors are represented by planes, and the coloring is the same. The main trend is that lethal metastases will be shed at smaller primary diameters when α is large.

The end combination of values chosen for the fits given in Table 1 is the one that roughly maximizes the correlation with both metrics. This is where μ_v is large and α is large for the lung tumor fit and where μ_v is small and α is small for the breast tumor fit.

Discussion

The combined model approach presented here bridges a broad population-level perspective with a dynamic tissue-level perspective. This method helps to resolve the differences at the tissue level between cancers with large differences in growth dynamics inferred at the population level, such as lung and breast cancer. The coupling of the 2 models is facilitated by the use of CTCs, but critically, it is the incorporation of a dynamic vascular response that provides a means to capture the observed differences in progression.

Much observation, theory, and speculation has led to different ideas on how a tumor grows (1, 13). Variation is inevitable considering the many different types of cancer, the multitude of causes, genetic and environmental factors, different time points and phases at observation, etc. Researchers have reported tumor growth characterized as linear (14, 15), exponential (16, 17), power law (18, 19), logistic (20), and Gompertzian (21). In the end, the equation specifics may not matter unless it changes the description of the dynamics and in turn the predictive power of the model.

The population-level stochastic model predicts exponential growth for the metastatic burden, so an exponential was used to fit the primary tumor as well. However, several different curves may be fit to the primary tumor to get good correlation. An investigation of the tissue-scale PDE model reveals that the

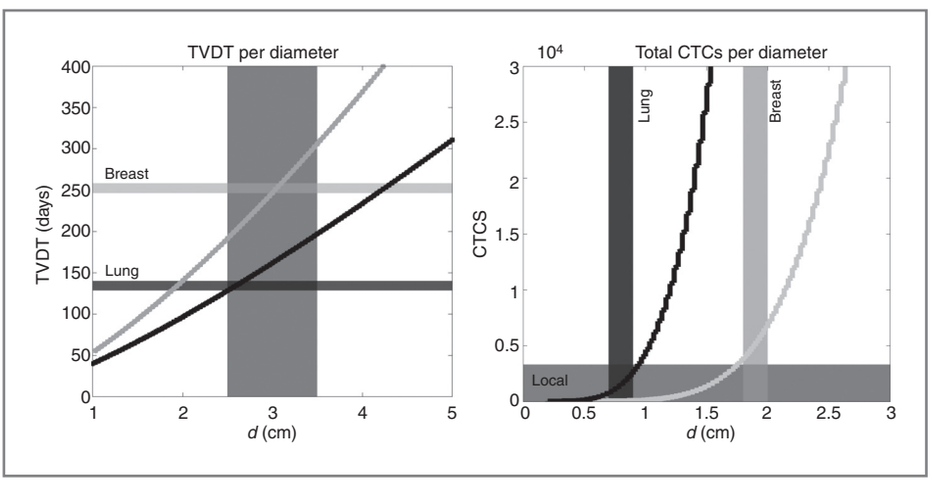

Figure 5. The 2 metrics for correlating the models: TVDT and number of CTCs. The latter is associated with the metastatic burden. The leftmost graph shows the TVDT (via Eq. 2s in Supplementary Data) per diameter of the tumor. The horizontal lines mark the estimates from the statistical population model for the breast (light) and the lung (dark). The vertical gray box sets a window for TVDT correlation with a ~3 cm tumor. The graph to the right shows the number of CTCs over time for lung (dark) and breast (light), found by keeping count of the cells that leave the primary at each time step.

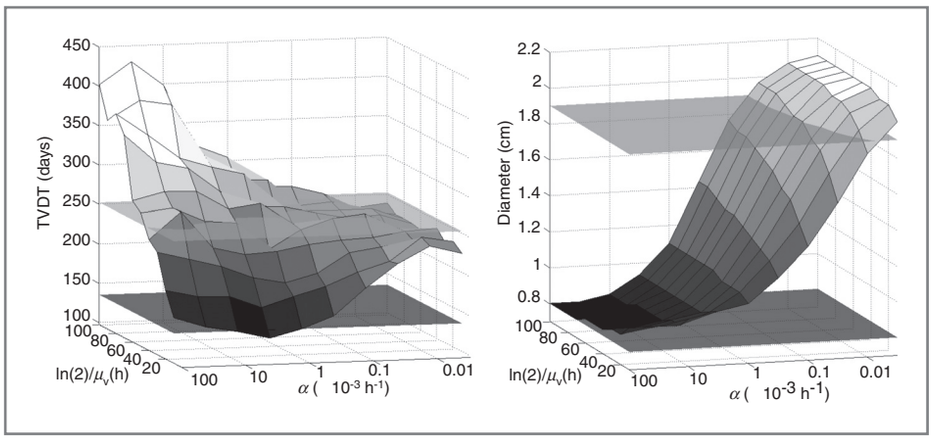

Figure 6. The left panel shows the TVDT at 3 cm diameter (via Eq. 2s in Supplementary Data) over an array of values for μ_v and α. The horizontal planes appear at the median values of 252 and 135 days for breast (light) and lung (dark), respectively. The right panel shows the primary tumor diameter upon reaching the threshold 3,300 CTCs over an array of values for μ_v and α. The horizontal planes appear at the median values of 1.9 and 0.8 cm for breast (light) and lung (dark), respectively.

primary tumor may grow exponentially or as a power law depending on the vascular dynamics. It is found that the vascular response must be large to sustain an exponentially growing primary tumor and slows toward power law growth otherwise. By disconnecting the growth of the primary from the growth of the CTCs, we allow a varied set of growth laws to encapsulate the primary, whereas the metastatic burden may still grow exponentially. The differences in growth occur with different relative populations of cell types, most notable are the vascular density and the hypoxic and normoxic fractions.

The vascular density contrasts markedly between breast and lung (cf. Fig. 3), with portions of the tissue of around 5% and 50%, respectively. A sample of histological measurements using various metrics is compiled from the literature in Table 2, to check for this divergence. All of the values have been converted to percentages so that they can be compared. The first 2 metrics show a larger proportion of vasculature in lung over breast and support our findings. In these comparisons either measurements from both lung tumors and breast tumors are given from the same group or the method is consistent across groups (Chalkley). With the highest microvessel count, however, the breast tumor is seen to have the higher fraction, which contradicts our findings. But in this case, each measurement is given by a different group with slightly different methods, the conversion from a count to a percent assumes the same average vessel size (which may not be valid), and perhaps while the average values are different, the vasculature may reach a saturation so that the highest microvessel counts are actually quite similar (in which case the results might be correct but not relevant). The last 3 metrics do not have measures for both lung and breast, so with the incomplete information we are unable to compare them.

Although the table shows some indication that lung tumors may be more vascular, it also points out the great diversity of quantities caused by a lack of common measure. Although microvascular density (MVD) for lung has been reported as not significant for prognosis (22), a Chalkley cutoff of 7 (~28%) for breast has good prognostic value (23). Given these contrasting trends by a multitude of measurements, it is unconvincing whether the degree of vascularity alone is a good predictor for progression. However, it is well accepted that that the vasculature is densest at the periphery of the tumor (6, 24, 25), which is seen in the simulated tumors as a peak vascular density close to the tumor–tissue interface.

In the tissue model, the proportions of normoxic and hypoxic cells are also quite different from lung tumor to breast tumor. The smaller vascular response of the breast tumor correlates with a dominant normoxic fraction, and the larger vascular response coexists with a dominant hypoxic fraction in lung. The hypoxic cells are ultimately the source of stimulation for vasculature. So it may seem counterintuitive to suggest that a lung tumor is both more vascular and more hypoxic than a breast tumor, but it is, in fact, the lack of vasculature that

Table 2. Measurements of vasculature content using various methods collected from the literature

Vascularity measurement	Mean % (range)	
	Breast	Lung
Chalkley[a]	20 (11–48)	28 (12–60)
	21.5 (8.0–44.0)	
	23.0 (9.3–32.0)	
	23.0 (8.0–47.0)	
MVD[b]	4.8 (1.1–22.7)	7.9 (3.4–35.0)
HMC[b]	2.7 (0.7–8.4)	2.5 (0.60–5.3)
	3.6 (0.9–7.3)	
AMC[b]	1.7 (0.1–4.2)	
VA/TA[c]		2.7 (2.0–3.8)
BV/TV[d]		6.6 (2.6–9.0)

NOTE: Values have been converted, as specified by the footnotes, to be expressed as a percentage from the details given in the cited references.

[a]Chalkley, counts were divided by 25 to get a percentage (23, 26–28).

[b]MVD/AMC/HMC, microvascular density, average, and highest microvessel count converted by assuming mean vessel radius is 10 μm and taking into account the size of the field in which the count was taken (26, 27, 29, 30, 31).

[c]VA/TA, vessel area/tumor area (32).

[d]BV/TV, blood volume/tumor volume (33).

stimulates the call for more. The presence of a large density of hypoxic cells is significant, as emerging evidence implicates hypoxia as a key inducer of angiogenesis and metastasis in tumors (34). As stated previously, an increased vasculature in the tumor periphery usually correlates with advanced disease, but when it is in conjunction with high VEGF levels (hypoxic), the advancement is more pronounced (24). This implies that the presence of both vasculature and hypoxia leads to more aggressive tumors, which is what we observe with this model. Hypoxic cells are also less sensitive to both radiation and chemotherapy (35, 36), so choice of treatment is affected by a tumor's oxygen profile (37).

The relative values of cell subtypes are dependent on the interaction rates between the cell compartments. In the tissue model, this difference is brought about by 2 main parameters: the vascular doubling time (μ_v) and the normoxia–hypoxia exchange rates (α). It is not surprising that increasing the rate of proliferation of endothelial cells will lead to a faster TVDT because a limited vasculature is the main limit on the growth, but the significance of the normoxia–hypoxia conversion rates is not immediately clear. The hypoxic compartment must be populated to keep the vasculature turning over, so we take a closer look at the total hypoxic turnover (2nd equation in Eq. A). Using the derivation and assumptions in Supplementary Data Appendix 4, we solve for the vascular density:

$$\nu \approx \frac{1-\sigma(\delta_h/\alpha_h)}{1+\sigma} \tag{3}$$

where $\sigma = \alpha_h h/\alpha_n n$ represents the rate toward reoxygenation over the rate toward deoxygenation. When $\sigma > 1$, there is a net reoxygenation, when $\sigma < 1$, there is a net deoxygenation, and when $\sigma = 1$, there is no net flux to either the hypoxic or normoxic compartment.

For the lung tumor α_h is very large, so we end up with $\nu \sim 1/(1+\sigma)$. The σ term approaches 1 for the lung tumor interior, so this gives a vascular content of 50%, which is what we indeed observe in Fig. 3. For the breast tumor, α_h is much smaller, so the second term in the numerator is significant. Also, α_h is slightly smaller than δ_h, so to ensure that the numerator is not negative, σ must be less than one. We observe that this is the case because the normoxic population is greater than the hypoxic population for the breast tumor. The end effect is that this term significantly reduces the numerator and makes the vasculature much smaller for the breast tumor (~5%). We also see that the effect of δ_h on the model system is captured in Eq. 3. As the rate of entry into the necrotic compartment is increased, the growth of the primary slows. The reason is that if more of the hypoxic fraction goes into the irreversible necrotic state, it is not present to attract the vasculature.

It turns out that the breast tumor slowly feeds the hypoxic fraction with a small and positive net hypoxic turnover rate throughout, whereas the lung tumor has a large hypoxic turnover at the leading edge, but shifts to a slight reoxygenation in the interior of the tumor. This leads to a maximal growth rate, with an optimized ratio of normoxic to hypoxic cells ($\sigma = 1$). The left panel of Fig. 6 emphasizes that there is mainly one way to grow maximally, but slowing the growth can be accomplished in a variety of ways. Although this result is based mainly on the mathematics of the system, there may be a physical and biological basis. Chaudary and Hill suggest that mechanisms may exist to promote the invasiveness of acutely hypoxic cells (38), so there's a parallel where switching between compartments may promote more aggressiveness than a gradual shift to hypoxia.

The parameter α also affects the growth of the CTCs indirectly through the vasculature. The CTC growth equation is the fourth equation in Eq. A. Because the entry rates into the circulation from either compartment (β_n and β_h) are of the same order of magnitude, CTC growth ultimately depends on the vasculature. The larger α associated with the lung tumor leads to about 10 times the vasculature and therefore a faster growing CTC population.

There has been considerable effort and an increased popularity in isolating, identifying, and characterizing cancer cells in the bloodstream for diagnosis and prognosis especially as assay reliability increases (10–12, 39–41). CTC assays rely on identifying cells epithelial in origin to those hematopoietic in origin. The frequency of these cells in metastatic patients occur on the order of approximately 1 CTC per 10^5–10^8 mononuclear cells and even lower in patients with localized cancer (39, 42, 43). A typical estimate for a threshold of poor prognosis from these references and the number used for the curve fitting is 5 CTCs per 7.5 mL of blood, although some estimates may be up to 38 CTCs in an equivalent volume (8). Even a single CTC detected in 7.5 mL of blood may be associated with the development of lethal metastases (40), and many cells may be present that are not tumorigenic (43). What happens to the CTCs once they have left the primary tumor does not feed back to the primary tumor, so considering death or fractional tumorigenicity of CTCs is a simple scaling of the population modeled here. It is clear that the error involved is large, but no matter where the threshold line is drawn, it does not change the underlying interactions and dynamics.

In this model, we have coarsely discriminated between fast and slow-growing tumors that shed metastases at small and large sizes, respectively. The results here suggest that tumor growth is ideally exponential. A less than sufficient angiogenic support system, however, leads to power law growth. It is not a simple scaling to relate a primary tumor with power law growth to metastases that grow exponentially. The CTCs, as an intermediary, disconnects the populations to bridge the scales using measurements we can observe.

We find that the breast tumor grows slower, has a minimal vascular density, a very large normoxic population, and a slow-growing CTC population. In contrast, the lung tumor grows faster, has a very large vascular density, a hypoxic population that is slightly larger than the normoxic population, and a much faster growing CTC population. Because of the differences in vascular response, the progression of these 2 tumors is quite different. Lung tumors have a greater risk of fatal metastatic burden at small sizes, whereas a breast tumor diagnosed at a larger size, may still be considered confined to the primary site. Perhaps knowing the CTC count when there's a highly vascular primary lung tumor might indicate the level of progression, but also finding a larger CTC count than expected when the

primary is a breast tumor might indicate that it is especially aggressive and should undergo alternative treatment. Therefore, CTC counts should be considered in an organ-specific manner and their importance weighted accordingly.

Bridging population-scale measurements from the SEER database down to the tissue-scale dynamics has been achieved through the use of two distinct mathematical modeling approaches. By matching tumor volume doubling time and metastatic burden across these scales, we have already gained significant understanding of the differences between breast and lung cancer. It is clear is that if we were able to obtain more detailed histological attributes of a patient's primary cancer, we could make even better predictions with our approach. Ultimately, this highlights a limitation and therefore a need in databases such as SEER to incorporate as much information about a given patient's tumor at the tissue level as possible, such as distributions of vasculature, necrosis, hypoxia, etc. of the primary and secondary tumors, as well as CTC counts (as technology develops). In addition, this endeavor has taught us the power of bridging multiple scales with different models and opens a new and exciting line of inquiry in our quest to better explain and predict cancer growth and progression.

Disclosure of Potential Conflicts of Interest

No potential conflicts of interest were disclosed.

Authors' Contributions

Conception and design: J. Gallaher, S. Plevritis, A.R.A. Anderson
Development of methodology: J. Gallaher, A. Babu, S. Plevritis, A.R.A. Anderson
Acquisition of data (provided animals, acquired and managed patients, provided facilities, etc.): S. Plevritis
Analysis and interpretation of data (e.g., statistical analysis, biostatistics, computational analysis): J. Gallaher, A. Babu, S. Plevritis
Writing, review, and/or revision of the manuscript: J. Gallaher, S. Plevritis, A.R.A. Anderson
Administrative, technical, or material support (i.e., reporting or organizing data, constructing databases): S. Plevritis
Study supervision: S. Plevritis, A.R.A. Anderson

Acknowledgments

The authors gratefully acknowledge funding from the Integrative Cancer Biology Program (ICBP) and the Cancer Intervention and Surveillance Network (CISNET) at the National Cancer Institute, through grants 1R01CA105366, 1U01CA088248, NIH U01CA159256, U54CA149145, U54CA113007, and U01CA151924.

The costs of publication of this article were defrayed in part by the payment of page charges. This article must therefore be hereby marked *advertisement* in accordance with 18 U.S.C. Section 1734 solely to indicate this fact.

Received March 13, 2013; revised September 4, 2013; accepted October 9, 2013; published OnlineFirst xx xx, xxxx.

References

1. Gerlee P. The model muddle: in search of tumor growth laws. Cancer Res 2013;73:2407–11.
2. SEERStat* Surveillance, Epidemiology, and End Results (SEER) Program (www seer cancer gov);. SEER*Stat Database: Incidence - SEER 17 Regs Limited - Use? Hurricane Katrina Impacted Louisiana Cases, Nov 2007 Sub (1973-2005 varying) - Linked To County Attributes - Total U.S., 1969-2005 Counties, National Cancer Institute, DCCPS, Surveillance Research Program, Cancer Statistics Branch, released April 2008, based on the November 2007 submission.
3. Lin RS, Plevritis SK. Comparing the benefits of screening for breast cancer and lung cancer using a novel natural history model. Cancer Causes Control 2012;23:175–85.
4. Swanson KR, Rockne RC, Claridge J, Chaplain MA, Alvord EC Jr, Anderson AR. Quantifying the role of angiogenesis in malignant progression of gliomas: *in silico* modeling integrates imaging and histology. Cancer Res 2011;71:7366–75.
5. Hinow P, Gerlee P, McCawley LJ, Quaranta V, Ciobanu M, Wang S, et al. A spatial model of tumor-host interaction: application of chemotherapy. Math Biosci Eng 2009;6:521–46.
6. Dvorak HF. Rous-whipple award lecture: how tumors make bad blood vessels and stroma. Am J Pathol 2003;162:1747–57.
7. Weidner N. New paradigm for vessel intravasation by tumor cells. Am J Pathol 2002;160:1937–9.
8. Hofman V, Bonnetaud C, Ilie MI, Vielh P, Vignaud JM, Fléjou JF, et al. Preoperative circulating tumor cell detection using the isolation by size of epithelial tumor cell method for patients with lung cancer is a new prognostic biomarker. Clin Cancer Res 2010;17:827–35.
9. Eschwège P, Moutereau S, Droupy A, Douard R, Gala JL, Benoit G, et al. Prognostic value of prostate circulating cells detection in prostate cancer patients: a prospective study. Br J Cancer 2009;100:608–10.
10. Cristofanilli M, Budd GT, Ellis MJ, Stopeck A, Matera J, Miller MC, et al. Circulating tumor cells, disease progression, and survival in metastatic breast cancer. N Engl J Med 2004;351:781–91.
11. Budd GT, Cristofanilli M, Ellis MJ, Stopeck A, Borden E, Miller MC, et al. Ciculating tumor cells versus imaging—predicting overall survival in metastatic breast cancer. Clin Cancer Res 2006;12:6403–9.
12. Liu MC, Shields PG, Warren RD, Cohen P, Wilkinson M, Ottaviano YL, et al. Circulating tumor cells: a useful predictor of treatment efficacy in metastatic breast cancer. J Clin Oncol 2009;27:5153–9.
13. Nakasu S, Nakasu Y, Fukami T, Jito J, Nozaki K. Growth curve analysis of asymptomatic and symptomatic meningiomas. J Neurooncol 2011;102:303–10.
14. Mayneord WV. On the law of growth of Jensen's rat sarcoma. Cancer Res 1932;16:841–6.
15. Schrek R. A comparison of the growth curves of malignant and normal (embryonic and postembryonic) tissues of the rat. Am J Pathol 1936;12:525–30.
16. Steel GG, Lamerton LF. The growth rate of human tumors. Br J Cancer 1966;20:74–86.
17. Peer PGM, van Dijck JAAM, Hendriks JHCL, Holland R, Verbeek ALM. Age-dependent growth rate of primary breast cancer. Cancer 1993;71:3547–51.
18. Hart D, Shochat E, Agur Z. The growth law of primary breast cancer as inferred from mammography screening trials data. Br J Cancer 1998;78:382–7.
19. Gatenby RA, Frieden BR. Inducing catastrophe in malignant growth. Math Med Biol 2008;25:267–83.
20. Weedon-Fekjaer H, Lindqvist BH, Vatten LJ, Awlen OO, Tretli S. Breast cancer tumor growth estimated through mammography screening data. Breast Cancer Res 2007;10:R41.
21. Laird AK. Dynamics of tumour growth. Br J Cancer 1964;18:490–502.
22. Trivella M, Pezzella F, Pastorino U, Harris AL, Altman DG. Microvessel density as a prognostic factor in non-small-cell lung carcinoma: a meta-analysis of individual patient data. Lancet Oncol online 2007;8:488–99.
23. Dhakal HP, Naume B, Synnestvedt M, Borgen E, Kaaresen R, Schlichting E, et al. Vascularization in primary breast carcinomas: its prognostic significance and relationship with tumor cell dissemination. Clin Cancer Res 2008;14:2341–50.
24. Ushijima C, Tsukamoto S, Yamazaki K, Yoshino I, Sugio K, Sugimachi K. High vascularity in the peripheral region of non-small cell lung cancer tissue is associated with tumor progression. Lung Cancer 2001;34:233–41.
25. Dagnon K, Heudes D, Bernaudin JF, Callard P. Computerized morphometric analysis of microvasculature in non-small cell lung carcinoma. Microvasc Res 2008;75:112–8.
26. Offersen BV, Pfeiffer P, Hamilton-Dutoit S, Overgaard J. Patterns of angiogenesis in non-small cell lung carcinoma. Cancer 2001;91:1500–9.

27. Offersen BV, Sørenson FB, Yilmaz M, Knoop A, Overgaard J. Chalkley estimates of angiogenesis in early breast cancer. Acta Oncol 2002; 41:695–703.
28. Offersen BV, Borre M, Overgaard J. Quantification of angiogenesis as a prognostic marker in human carcinomas: a critical evaluation of histopathological methods for estimation of vascular density. Eur J Cancer 2003;39:881–90.
29. Takei H, Iino Y, Horiguchi J, Maemura M, Nagaoka H, Koibuchi Y, et al. Highest microvessel count as a long-term prognostic factor in Japanese breast cancer patients. Cancer Lett 2000;156:109–16.
30. Kang YH, Kim KS, Yu YK, Lim SC, Kim YC, Park KO. The relationship between microvessel count and the expression of vascular endothelial growth factor, p53, and K-ras in non-small cell lung cancer. J Korean Med Sci 2001;16:417–23.
31. Kato T, Steers G, Campo L, Roberts H, Leek RD, Turley H, et al. Prognostic significance of microvessel density and other variables in Japanese and British patients with primary invasive breast cancer. Cancer Res UK 2007;97:1277–86.
32. Zhang L, Yankelevitz DF, Henschke CI, Reeves AP, Vazquez MF, Carter D. Variation in vascular distribution in small lung cancers. Lung Cancer 2010;68:389–93.
33. Ng QS, Goh V, Milner J, Sundin J, Wellsted D, Saunders MI, et al. Quantitative helical dynamic contrast enhanced computed tomography assessment of the spatial variation in whole tumour blood volume with radiotherapy in lung cancer. Lung Cancer 2010;69:71–6.
34. Park JE, Tan HS, Datta A, Lai RC, Zhang H, Meng W, et al. Hypoxic tumor cell modulates its microenvironment to enhance angiogenic and metastatic potential by secretion of proteins and exosomes. Mol Cell Proteomics 2010;9:1085–99.
35. Vaupel P, Kallinowski F, Okunieff P. Blood flow, oxygen and nutrient supply, and metabolic microenvironment of human tumors: a review. Cancer Res 2006;49:6449–65.
36. Crosse JP, Michiels C. Tumour hypoxia affects the responsiveness of cancer cells to chemotherapy and promotes cancer progression. Anticancer Agents Med Chem 2008;8:790–7.
37. Brown JM, Wilson WR. Exploiting tumor hypoxia in cancer treatment. Nat Rev Cancer 2004;4:437–47.
38. Chaudary N, Hill RP. Hypoxia and metastasis. Clin Cancer Res 2007;13:1947–9.
39. Allan AL, Keeney M. Circulating tumor cell analysis: technical and statistical considerations for the application to the clinic. J Oncol 2009;2010:1–10.
40. Bidard FC, Mathiot C, Delaloge S, Brain E, Giachetti S, de Cremoux P, et al. Single circulating tumor cell detection and overall survival in nonmetastatic breast cancer. Ann Oncol 2010;21:729–33.
41. Cen P, Ni X, Yang J, Graham DY, Li M. Circulating tumor cells in the diagnosis and management of pancreatic cancer. Biochem Biophys Acta 2012;1826:350–6.
42. O'Flaherty JD, Gray S, Richard D, Fennell D, O'Leary JJ, Blackhall FH, et al. Circulating tumour cells, their role in metastasis and their clinical utility in lung cancer. Lung Cancer 2012;76:19–25.
43. Doyden J, Alix-Panabières C, Hofman P, Parks SK, Chamorey E, Naman H, et al. Circulating tumor cells in prostate cancer: a potential surrogate marker of survival. Crit Rev Oncol Hemotol 2012;81:241–56.
44. Bray D. Cell movements. vol. 467. New York: Garland Publishing; 1992.
45. Pennacchietti S, Michieli P, Galluzzo M, Mazzone M, Giordano S, Comoglio PM. Hypoxia promotes invasive growth by transcriptional activation of the *met* protooncogene. Cancer Cell 2003;3:347–61.
46. Anderson ARA, Chaplain MAJ. Continuous and discrete mathematical models of tumor-induced angiogenesis. Bull Math Biol 1998;60: 857–99.
47. Orme ME, Chaplain MAJ. A mathematical model of vascular tumour growth and invasion. Math Comput Model 1996;23:43–60.
48. Tyson DR, Garbett SP, Frick PL, Quaranta V. Fractional proliferation: a method to deconvolve cell population dynamics from single cell data. Nat Methods Advance Online Publication. 2012;9:923–8.
49. Anderson ARA, Hassanein M, Branch KM, Lu J, Lobdell NA, Maier J, et al. Microenvironmental independence associated with tumor progression. Cancer Res 2009;69:8797–806.
50. Hobson B, Denekamp J. Endothelial proliferation in tumours and normal tissues: continuous labelling studies. Br J Cancer 1984;49: 405–13.
51. Ljungkvist ASE, Bussink J, Rijken P, Kaanders JHAM, van de Kogel AJ, Denekamp J. Vascular architecture, hypoxia, and proliferation in first-generation xenografts of human head-and-neck squamous cell carcinomas. Int J Radiat Oncol Biol Phys 2002;54:215–28.
52. Lanzen J, Braun RD, Klitzman B, Brizel D, Secomb TW, Dewhirst MW. Direct demonstration of instabilities in oxygen concentrations within the extravascular compartment of an experimental tumor. Cancer Res 2006;66:2219–23.
53. Benjamin LE, Golijanin D, Itin A, Pode D, Keshet E. Selective ablation of immature blood vessels in established human tumors follows vascular endothelial growth factor withdrawal. J Clin Invest 1999;103:159–65.
54. Durand RE, Sham E. The lifetime of hypoxic human tumor cells. Int J Radiat Oncol Biol Phys 1998;42:711–5.
55. Ljungkvist ASE, Bussink J, Kaanders JHAM, Rijken PFJW, Begg AC, Raleigh JA, et al. Hypoxic cell turnover in different solid tumor lines. Int J Radiat Oncol Biol Phys 2005;62:1157–68.
56. Vaupel P. Metabolic microenvironment of tumor cells: a key factor in malignant progression. Exp Oncol 2010;32:125–7.